High-Resolution PET in Cats: Application of a Clinical Camera to Experimental Studies

W.-D. Heiss, K. Wienhard, R. Graf, J. Löttgen, U. Pietrzyk and R. Wagner

Max-Planck-Institut für Neurologische Forschung, Neurologische Universitätsklinik, Köln, Germany

A commercial high-resolution scanner designed for clinical PET studies was tested for its applicability to investigate cerebral metabolism and blood flow in cats. **Methods:** Cerebral blood flow, $CMRO_2$, CBV and CMR_{glc} were determined repeatedly using ^{15}O steady-state oxygen methods and ^{18}F-fluorodeoxyglucose (FDG). Metabolic and blood flow images of 14 contiguous 3-mm PET slices were compared to histological sections in four control animals. In another six cats, hemodynamic and metabolic changes were followed by serial multi-tracer PET for 24 hr after permanent occlusion of the left middle cerebral artery (MCA). Pattern and extent of changes of the physiological variables were related to the final infarct verified in matched histological sections. **Results:** At spatial resolutions (FWHM) of 3.6 mm in transaxial planes and 4.0 mm axially, details of the gross anatomy of the cat brain were distinguished best in the FDG images. Cerebral blood flow, $CMRO_2$ and CMR_{glc} values measured in the cortex, white matter and basal ganglia were in the range of common autoradiographic results. Immediately after MCA occlusion, there was widespread decrease in blood flow, but metabolism was preserved at values, which suggest viable tissue. With time, the areas of increased oxygen extraction fraction (OEF) moved from the center to the periphery of the MCA territory. **Conclusion:** High-resolution PET can be used for repeat, quantitative imaging of blood flow and metabolism in small animals such as the cat. After MCA occlusion, the changes in blood flow and metabolism can be followed over time and can be related to the final morphological lesion.

Key Words: high-resolution PET; quantitative imaging; blood flow

J Nucl Med 1995; 36:493–498

Autoradiography has been the most important and widely applied method for measuring regional cerebral blood flow (*1,2*) and metabolism (*3*) in experimental research. The transfer to nuclear medicine applications of models and methods initially developed for autoradiography has allowed the determination of physiological variables in man in many instances. PET, in particular, has benefited from these concepts and is often referred to as in vivo autoradiography or physiological tomography (*4*). Despite these relationships, there still exists a large discrepancy between the results obtained at well-defined but singular time points in the course of an experiment, and the data acquired incidentally at varying time points in the course of clinical disorders. Furthermore, important physiological variables, e.g., oxygen consumption, cannot be assessed quantitatively by conventional experimental imaging techniques.

Previous PET studies in animals were used mainly to analyze the biodistribution and kinetics of new tracers developed for PET (*5–8*) and to follow the distribution of tracers in the brain, especially in areas with high-selective uptake and specific tracer binding, e.g., dopaminergic tracers (*9–14*) and benzodiazepine receptor ligands (*15,16*). Other animal studies dealt with the brain uptake of labeled drugs and its inhibition. For example, the latter kind of study was performed with labeled MPTP and the specific blockade of its brain uptake by MAO-B inhibitors (*17*). Mainly because of limitations with spatial resolution, physiological variables of animals under normal conditions were rarely studied with PET tracer methodologies. Only a rough correlation of selected regions of interest (ROIs) with anatomical structures was achieved (*18*). In a few instances, the altered uptake of tracers was demonstrated in experimental lesions, e.g., in focal edema following cold injury (*19*) or after thromboembolic stroke (*20*). Experimental investigations also utilized the specific changes of receptor binding of radioligands in relation to brain damage of varying degree, e.g., in graded ischemia (*21*). Systematic investigations of altered physiology in acute experimental conditions like focal cerebral ischemia were limited by poor spatial resolution and were performed only in a few instances (*22*), yielding rather global results.

In several institutions, PET scanners were customized for application to animals (*9,10,23*). With the advent of a new generation of commercial PET machines for clinical purposes, featuring high-spatial resolution in all dimensions, several physiological variables can now be imaged quantitatively even in smaller animals like the cat. Therefore the regional data can be related to normal morphology or pathoanatomy.

METHODS

Ten adult cats of both sexes, weighing 2.5 kg to 3.6 kg, were anesthetized with ketamine hydrochloride (25 mg/kg i.m.), trache-

Received Mar. 29, 1994; revision accepted Aug. 8, 1994.

For correspondence or reprints contact: Prof. Dr. W.-D. Heiss, MPI f. neurol. Forschung, Gleueler Str. 50, D-50931 Köln, Germany.

ostomized, immobilized with pancuronium bromide (0.2 mg/kg i.v.), and artificially ventilated. Anesthesia was continued with 0.8%–1.5% halothane in a 70% N_2O/30% O_2 gas mixture. Physiological variables were kept in the normal range for awake cats; deep body temperature was maintained at 37°C to 37.5°C. Four animals were studied repeatedly without further surgical procedures and served as controls. In six cats, the left MCA was exposed transorbitally and an implanted device (*24*) was used to occlude the MCA with a microdrive through the resealed orbit.

Each cat underwent multiple consecutive PET studies. In animals with MCA occlusion, control measurements before and up to six measurements after occlusion were performed over an experimental period of 24 hr. For that purpose, cats were positioned with a head holder in the scanner gantry. Comparability among animals was achieved by the numerous 3.1 mm coronal tomographic slices across the cat's head, comprising the whole brain and permitting three-dimensional reconstruction and alignment to histological sections obtained in the same orientation. Correction of photon attenuation was carried out in each cat, using a transmission scan performed with rotating ^{68}Ge rod sources. For the assessment of cerebral blood flow (CBF), cerebral metabolic rate for oxygen ($CMRO_2$), oxygen extraction fraction (OEF), and cerebral blood volume (CBV) the steady-state ^{15}O continuous inhalation method (*25*) was used with successive inhalations of tracer amounts of $C^{15}O_2$, $^{15}O_2$ and $C^{15}O$. Cerebral glucose metabolic rate (CMR_{glc}) was measured after injection of 2 mCi ^{18}F-2-fluoro-2-deoxy-D-glucose (FDG) (*26*).

Serial PET scanning was performed with a CTI Siemens ECAT EXACT HR tomograph, a commercial, clinical PET system that provides high-spatial resolution. It consists of 24 detector rings equipped with 784 crystals each, covering an axial field of view (FOV) of 15 cm, which is divided into 47 contiguous image planes. Its properties and performance have been described previously (*27*). The facial dimension of the individual crystals is 5.9 × 2.9 mm^2, thus yielding, at the center of the FOV, a resolution of 3.6 mm transaxially and 4.0 mm axially. By limiting data acquisition to straight planes, i.e., only coincidences between opposing crystals in the same detector ring are being recorded, axial resolution can be improved to 3.5 mm.

Total count rates collected for $C^{15}O_2$ and $^{15}O_2$ studies ranged from 50.000 to 75.000 cps in 10 min frames, with transaxial slices being reconstructed from 1 to 1.5 million true coincidence counts per slice. For FDG studies, a total of 10^8 counts were collected over a 40 min period starting at 20 min after injection, permitting the reconstruction of transaxial slices from 4 million counts per slice. During each $C^{15}O_2$, $^{15}O_2$ and $C^{15}O$ scan, two arterial blood samples were taken (at the beginning and at the end of acquisition) for determination of blood gases and for whole blood and plasma radioactivity measurements in a well counter cross-calibrated to the camera. Their mean value was used for parametric image generation. During the FDG studies, eight blood samples were taken starting at tracer injection. Plasma radioactivity was used for CMR_{glc} calculations according to the model equation (*26*). Furthermore, plasma glucose concentrations were measured.

At the end of the experiment, the animals were perfusion fixed with formalin (4%) and the brains were removed. The occlusion of the MCA was verified and serial sections (stained with HE or Luxol Fast Blue) were matched individually with the various functional images to permit comparative assessment of infarcts. Data analysis was based on the parametric images from those 14 transaxial PET slices comprising the brain. For functional quantitation, circular regions of interest (ROIs, 5 mm in diameter) were placed in selected brain regions in relation to the corresponding histological sections. One set of ROIs was defined for each animal and was used for all studies of the same animal.

RESULTS

PET images of CBF, CBV, $CMRO_2$ and CMR_{glc} were obtained in four anesthetized cats without further surgery and in six animals after transorbital implantation of a device for occlusion of the middle cerebral artery. CBF and $CMRO_2$ images permitted the identification of the main anatomic, and CBV images of the main vascular structures within the cat's head. Optimum spatial resolution was afforded by the CMR_{glc} images, which permitted clear distinction, e.g., of caudate nucleus and olfactory bulb. As demonstrated in four selected slices across one cat's brain (Fig. 1), the functional images were in good agreement with the matched histological sections, permitting easy identification of specific structures in a stereotactic atlas (*28*). Despite the limited spatial resolution of the PET images compared to the size of a cat brain, physiological values could be obtained separately for compartments of mainly gray (cortex or basal ganglia) or white matter (Table 1). These values can serve as a basis for among- or within-animal comparisons in a variety of experiments. The highest values for CBF, $CMRO_2$ and CMR_{glc} were measured in ROIs containing large proportions of basal ganglia or cortex, while the lowest values were found in ROIs of mainly white matter. The ratio between cortex or basal ganglia and white matter values ranged between 1.4 and 2.0.

The capability of the PET system to distinguish regional pathophysiological changes was tested using the MCA occlusion model. In all six experimental animals, the arterial occlusion immediately reduced CBF to the respective supply territory below 30% of its control level, with a distinct but graded transition to surrounding brain tissue. Initially, $CMRO_2$ was less diminished, and consequently OEF was increased, thus indicating that oxygen supply was still sufficient to keep the tissue vital despite dense ischemia ("misery perfusion") (Fig. 2). In some cases, collateral circulation caused hyperperfusion outside the ischemic MCA territory and even in the contralateral hemisphere. In the core of ischemia, both $CMRO_2$ and OEF eventually decreased, suggesting necrotic tissue transformation. Over the next 4–6 hr, this process spread from the center of the MCA territory to the region adjoining the core of ischemia. In this border zone, blood flow was initially impaired to a lesser degree and $CMRO_2$ was preserved. Within 18–24 hr, MCA infarction became complete, with blood flow and energy metabolism being equally reduced. At that time, the size of the ultimate infarct was reflected best by CMR_{glc} images. However, because of the functional deactivation of anatomically preserved tissue in the close vicinity of the infarct, the areas of metabolic impairment were always slightly larger than the necrotic zone on histological sections. In animals with large infarcts, within 24 hr, the ensuing increase in intracranial pressure also impaired

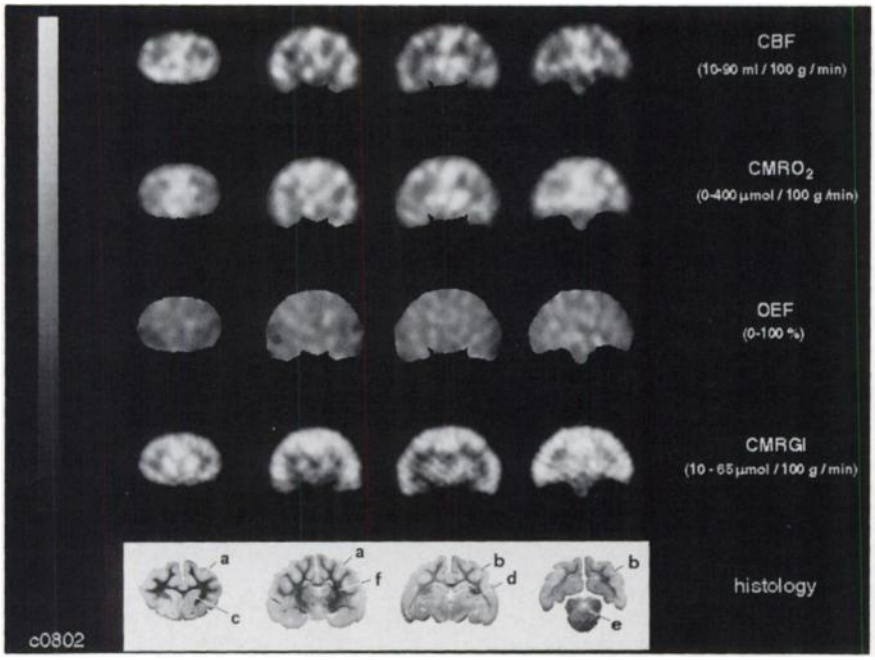

FIGURE 1. Matched transaxial tomographic brain sections at a 6-mm center-to-center slice distance show CBF, $CMRO_2$, OEF, CMR_{glc} (gray scale according to individual range) and histology of an anesthetized control cat. Anatomical details are well represented particularly in CMR_{glc} and $CMRO_2$ images. (a) Anterior cortex, (b) posterior cortex, (c) caudato putamen, (d) thalamus, (e) cerebellum/brainstem and (f) white matter.

blood flow of the contralateral hemisphere, and raised OEF indicated the development of whole-brain damage.

The quality of high-resolution PET images and the benefit of repeated multitracer studies is demonstrated by surface reconstructions of OEF (Fig. 3). In all cats, the ischemic penumbra, i.e., the area of increased OEF, spread with time from the center to the borders of the ischemic MCA territory. In most instances, that misery perfusion condition was followed by a marked OEF drop reflecting progressive impairment of blood flow and metabolism and suggesting transition to necrosis. While this dynamic penumbra in five cats indicated nothing but spread of infarction (Fig. 3, upper row), in one animal this condition was reversible and the involved cortex survived (Fig. 3, lower row). Eventually, this cat suffered only a small persistent ischemic lesion of basal ganglia and internal capsule.

DISCUSSION

The ECAT EXACT HR (*27*) has a spatial resolution of 3.6 mm in the plane of section and 4.0 mm axially at the center, which is slightly worse than the resolution obtained by pinhole SPECT (*29*). Therefore, the resolution capacity of the system is approximately 1/10 the dimension of a cat brain averaging 40 × 30 mm transaxially and 50 mm in the axial direction. Consequently, this scanner can be utilized with the described experimental model, as long as tracer concentrations are sufficient for imaging. Metabolism and blood flow values in gray matter are approximately 3–4 times higher than in white matter, thus permitting to distinguish gross anatomical structures: cat cerebral cortex has a thickness of only 1–2 mm, although it is folded into gyri and therefore appears thicker on images; basal ganglia and thalamus measure about 5–6 mm in diameter (*28,30*) and are easily detected. The low-energy positron emitted by ^{18}F and the abundance of counts available with the steady-state FDG method are the reasons why FDG images provide the best representation of anatomical detail. However, major structures can also be distinguished on blood flow and oxygen images. CBV images mainly show large vessels and basal structures and are useful for cor-

TABLE 1
PET Variables (means ± s.d., n = 4) in Various Brain Regions

Brain region	CBF (ml/100g/min)	CMRO2 (µmole/100g/min)	OEF (%)	CMRG1 (µmole/100g/min)	CBF (ml/100ml)
Cerebral cortex (anterior)	72 ± 6	396 ± 11	52 ± 4	60 ± 4	5.9 ± 0.5
Cerebral cortex (posterior)	75 ± 10	398 ± 11	52 ± 2	61 ± 5	5.7 ± 0.4
Caudoputamen	72 ± 5	383 ± 22	50 ± 3	6 ± 4	5.7 ± 0.6
Thalamus	67 ± 9	376 ± 21	48 ± 2	56 ± 8	5.8 ± 0.7
Cerebellum	60 ± 8	374 ± 15	55 ± 6	54 ± 4	5.7 ± 0.4
White matter (corona radiata)	33 ± 3	178 ± 11	48 ± 2	37 ± 3	4.1 ± 0.3

Three to four determinations in consecutive planes were averaged in each cat.

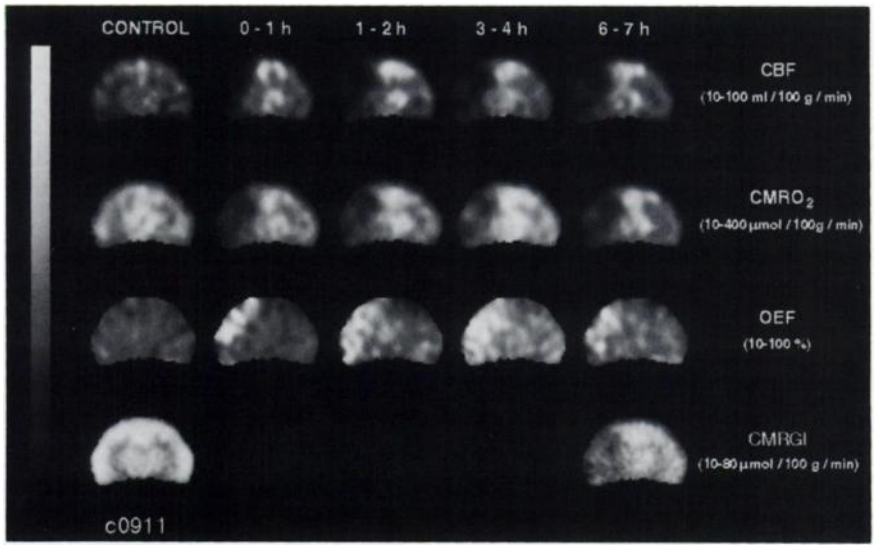

FIGURE 2. Matched transaxial slices in one plane at thalamic level before and at four time points after middle cerebral artery occlusion. CBF is severely decreased immediately after MCA occlusion, while $CMRO_2$ is partially preserved because of increased OEF. Gray scale according to individual range of values.

recting OEF estimates (*31*). Despite some inaccuracies related to partial volume effects (especially in white matter) the values calculated for the physiologic variables were close to those obtained by autoradiographic methods. Studies using autoradiography show values for CBF (*1,2,32*) and CMR_{glc} (*33,34*), comparable to our findings, with autoradiographic CBF estimates being slightly higher in gray and slightly lower in white matter (cortex, 75–130; striatum, 70–110; cerebellum, 55–110; white matter, 15–53 ml/100g/min). CMR_{glc} being almost identical, with the exception of a lower CMR_{glc} in white matter (cortex, 28–57; thalamus, 25–49; cerebellum, 45–54; white matter, 4–22 µmol/100g/min). Those differences between methods can be explained by partial volume effects and by the lower spatial resolution of PET. Compared to techniques necessitating tissue sampling, brain slicing, implantation of electrodes or detector probes for clearance recording (for review see 35), high-resolution PET as a regional method for repeated, noninvasive measurements of physiological variables has clear advantages for experimental research in medium-sized laboratory animals.

To date, only one PET study used ^{15}O-labeled tracers to investigate the changes with time of cerebral hemodynamics and metabolism early in the course of focal ischemia (*22*). Although a rather large experimental animal with a well-differentiated brain was chosen (baboon) anatomical resolution was quite limited. Furthermore, sequential PET scanning was not performed until the lesion had fully developed. Histological verification of pathoanatomical changes was not a major goal in the study. Our study demonstrates for the first time the correlation of matched PET images and histological sections, and makes use of serial multitracer PET scanning for the assessment of experimentally induced regional changes of blood flow and metabolism in a small, common laboratory animal. This technique was shown to be capable of closing the gap between high-resolution, quantitative experimental techniques like autoradiography and other biochemical imaging procedures (*34,36*) on one side, and the clinical functional imaging studies usually performed rather late in the course of acute human disease such as ischemic stroke (*37*) on the other. Most experimental imaging procedures require brain

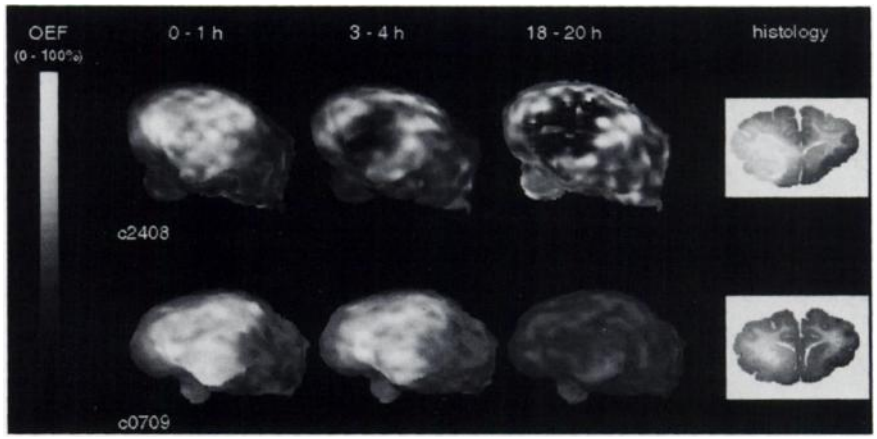

FIGURE 3. Lateral surface views of left hemisphere reconstructed from OEF. Upper row: increased OEF spreads with time from center to periphery of MCA territory and finally leads to large infarct, as seen in histology. Lower row: smaller subcortical infarct (histology) after transient increase in OEF during first 4 hr after MCA occlusion.

slicing and, therefore, can only be applied once. Moreover, imaging of oxygen consumption is still not feasible with the techniques generally applied in animal experiments.

High-resolution, serial PET scanning of tracers of perfusion and metabolism is still a unique approach to the regional pathophysiology leading to reversible or permanent ischemic brain damage. With respect to temporal resolution, this approach is inferior to advanced MR techniques especially designed for animal studies, e.g., diffusion-weighted and contrast-enhanced echo planar imaging which visualize changes early, fast, and repeatedly in the course of experimental focal ischemia (*38–41*). However, diffusion-weighted and contrast-enhanced MR images reflect parameters related to both perfusion and edema, and absolute quantitation of physiological variables is difficult. While resolution of experimental MRI is superior to PET, MR techniques in many fast, dynamic applications are still restricted to one slice of a thickness (1–6 mm, (*40–42*)) comparable to HR PET. Other MR techniques, especially spectroscopy, can be used for measuring the concentrations of selected biochemical substances (*43,44*). Therefore, PET and MR are not competitive but complementary modalities (*45*) in experimental research, each having its advantages and disadvantages. High-temporal and spatial resolution are the main attraction of some MR techniques, while comprehensive quantification of several physiological variables in many slices is the benefit of PET.

Considering the progress made in terms of spatial resolution, state-of-the-art PET can be applied to experimental research in cats, with a success rate similar to the application of PET in human studies in the early 1980s. During that period, important contributions to our knowledge of brain function and pathology came from low-resolution single-slice scanners. With advanced, high-resolution scanners permitting also three-dimensional data acquisition which provides sufficient counts even at low tracer concentrations, new insights into the pathophysiology of transient or permanent regional brain damage of different etiologies can be expected, and new therapeutic strategies can be evaluated in repeated imaging studies of relatively small experimental series.

REFERENCES

1. Landau WM, Freygang WH Jr, Rowland LP, Sokoloff L, Kety SS. The local circulation of the living brain: values in the unanesthetized and anesthetized cat. *Trans Am Neurol Assoc* 1955;80:125–129.
2. Sakurada O, Kennedy C, Jehle J, Brown JD, Carbin GL, Sokoloff L. Measurement of local cerebral blood flow with iodo(^{14}C)antipyrine. *Am J Physiol* 1978;234:H59–H66.
3. Sokoloff L, Reivich M, Kennedy C, et al. The (^{14}C)deoxyglucose method for the measurement of local cerebral glucose utilization: theory, procedure, and normal values in the conscious and anesthetized albino rat. *J Neurochem* 1977;28:897–916.
4. Phelps ME. PET: a biological imaging technique. *Neurochem Res* 1991;16: 929–940.
5. Hawkins RA, Huang SC, Barrio JR, et al. Estimation of local cerebral protein synthesis rates with L-(1-^{11}C)leucine and PET: methods, model, and results in animals and humans. *J Cereb Blood Flow Metab* 1989;9:446–460.
6. Fowler JS, Wolf AP. Recent advances in radiotracers for PET studies of the brain. In: Diksic M, Reba RC, eds. *Radiopharmaceuticals and brain pathology studied with PET and SPECT*. Boca Raton: CRC Press; 1991:11–34.
7. Stöcklin G. Tracers for metabolic imaging of brain and heart. *Eur J Nucl Med* 1992;19:527–551.
8. Ingvar M, Eriksson L, Rogers GA, Stone-Elander S, Widén L. Rapid feasibility studies of tracers for positron emission tomography: high-resolution PET in small animals with kinetic analysis. *J Cereb Blood Flow Metab* 1991;11:926–931.
9. Watanabe M, Uchida H, Okada H, et al. A high-resolution PET for animal studies. *IEEE Trans Med Imaging* 1992;11:577–580.
10. Rajeswaran S, Jones WF, Byars LG, et al. Physical characteristics of a small diameter positron emission tomograph. *IEEE Nucl Sci Symp Med Imaging Conference* 1992;985–987.
11. Ehrin E, Farde L, De Paulis T, et al. Preparation of ^{11}C-labelled raclopride, a new potent dopamine receptor antagonist: preliminary PET studies of cerebral dopamine receptors in the monkey. *Int J Appl Radiat Isot* 1985; 36:269–273.
12. Fowler JS, Arnett CD, Wolf AP, et al. A direct comparison of the brain uptake and plasma clearance of N-(^{11}C)methylspiroperidol and (^{18}F)N-methylspiroperidol in baboon using PET. *Nucl Med Biol* 1986;13:281–284.
13. Coenen HH, Wienhard K, Stöcklin G, et al. PET measurement of D2 and S2 receptor binding of 3-N-([2'-^{18}F] fluoroethyl)spiperone in baboon brain. *Eur J Nucl Med* 1988;14:80–87.
14. Barrio JR, Satyamurthy N, Huang SC, et al. 3-(2'-(^{18}F)fluoroethyl)-spiperone: in vivo biochemical and kinetic characterization in rodents, non human primates, and humans. *J Cereb Blood Flow Metab* 1989;9:830–839.
15. Comar D, Mazière M, Godot JM, et al. Visualization of ^{11}C-flunitrazepam displacement in the brain of the live baboon. *Nature* 1979;280:329–331.
16. Hantraye P, Kaijima M, Prenant C, et al. Central type benzodiazepine binding sites: a positron emission tomography study in the baboons brain. *Neurosci Lett* 1984;48:115–117.
17. Moerlein SM, Stöcklin G, Pawlik G, Wienhard K, Heiss W-D. Regional cerebral pharmacokinetics of the dopaminergic neurotoxin 1-methyl-4-phenyl-1,2,3,6-tetrahydropyridine as examined by positron emission tomography in a baboon is altered by tranylcypromine. *Neurosci Lett* 1986;66:205–209.
18. Pinard E, Mazoyer B, Verrey B, Pappata S, Crouzel C. Rapid measurement of regional cerebral blood flow in the baboon using ^{15}O-labeled water and dynamic positron emission tomography. *Med Biol Eng Comput* 1993;31: 495–502.
19. Prenen GHM, Go KG, Paans AMJ, et al. Positron emission tomographical studies of 1-^{11}C-acetoacetate, 2-^{18}F-fluoro-deoxy-D-glucose, and L-1-^{11}C-tyrosine uptake by cat brain with an experimental lesion. *Acta Neurochir (Wien)* 1989;99:166–172.
20. De Ley G, Weyne J, Demeester G, et al. Experimental thromboembolic stroke studied by positron emission tomography: immediate versus delayed reperfusion in fibrinolysis. *J Cereb Blood Flow Metab* 1988;8:539–545.
21. Sette G, Baron JC, Young AR, et al. In vivo mapping of brain benzodiazepine receptor changes by positron emission tomography after focal ischemia in the anesthetized baboon. *Stroke* 1993;24:2046–2058.
22. Pappata S, Fiorelli M, Rommel T, et al. PET study of changes in local brain hemodynamics and oxygen metabolism after unilateral middle cerebral artery occlusion in baboons. *J Cereb Blood Flow Metab* 1993;13:416–424.
23. Cutler PD, Cherry SR, Hoffman EJ, Digby WM, Phelps ME. Design features and performance of a PET system for animal research. *J Nucl Med* 1992;33:595–604.
24. Graf R, Kataoka K, Rosner G, Heiss W-D. Cortical deafferentation in cat focal ischemia: disturbance and recovery of sensory functions in cortical areas with different degrees of CBF reduction. *J Cereb Blood Flow Metab* 1986;6:566–573.
25. Frackowiak RSJ, Lenzi GL, Jones T, Heather JD. Quantitative measurement of regional cerebral blood flow and oxygen metabolism in man using ^{15}O and positron emission tomography: theory, procedure, and normal values. *J Comput Assist Tomogr* 1980;4:727–736.
26. Reivich M, Kuhl D, Wolf A, et al. The (^{18}F)fluorodeoxyglucose method for the measurement of local cerebral glucose utilization in man. *Circ Res* 1979;44:127–137.
27. Wienhard K, Dahlbom M, Eriksson L, et al. The ECAT EXACT HR: performance of a new high-resolution positron scanner. *J Comput Assist Tomogr* 1994;18:110–118.
28. Reinoso-Suárez F. *Topographischer hirnatlas der katze*. Darmstadt: Hrsg E Merck AG; 1961:74.
29. Weber DA, Ivanovic M, Franceschi D, et al. Pinhole SPECT: An approach to in vivo high-resolution SPECT imaging in small laboratory animals. *J Nucl Med* 1994;35:342–348.
30. Rockel AJ, Hioms RW, Powell TPS. The basic uniformity in structure of the neocortex. *Brain* 1980;103:221–244.

31. Lammertsma AA, Jones T. Correction for the presence of intravascular oxygen-15 in the steady-state technique for measuring regional oxygen extraction ratio in the brain: I. Description of the method. *J Cereb Blood Flow Metab* 1983;3:416–424.
32. Sokoloff L. Cerebral circulation, energy metabolism and protein synsthesis: general characteristics and principles of measurement. In: Phelps ME, Mazziotta JC, Schelbert HR, eds. *Positron emission tomography and autoradiography*. New York: Raven Press; 1986:1–7.
33. Ginsberg MD, Reivich M, Giandomenico A, Greenberg JH. Local glucose utilization in acute focal cerebral ischemia: local dysmetabolism and diaschisis. *Neurology* 1977;27:1042–1048.
34. Hossmann K-A, Mies G, Paschen W, et al. Multiparametric imaging of blood flow and metabolism after middle cerebral artery occlusion in cats. *J Cereb Blood Flow Metab* 1985;5:97–107.
35. Hossmann KA. Animal models of cerebral ischemia. 1. Review of literature. *Cerebrovasc Dis* 1991;1(suppl 1):2–15.
36. Ginsberg MD. Local metabolic responses to cerebral ischemia. *Cerebrovasc Brain Metab Rev* 1990;2:58–93.
37. Heiss W-D, Podreka I. Role of PET and SPECT in the assessment of ischemic cerebrovascular disease. *Cerebrovasc Brain Metab Rev* 1993;5: 235–263.
38. Bose B, Jones SC, Lorig R, Friel HT, Weinstein M, Little JR. Evolving focal cerebral ischemia in cats: spatial correlation of nuclear magnetic resonance imaging, cerebral blood flow, tetrazolium staining and histopathology. *Stroke* 1988;19:28–37.
39. Moseley ME, Cohen Y, Mintorovitch J, et al. Early detection of regional cerebral ischemia in cats: comparison of diffusion- and T2-weighted MRI and spectroscopy. *Magn Res Med* 1990;14:330–346.
40. Hamberg LM, Macfarlane R, Tasdemiroglu E, et al. Measurement of cerebrovascular changes in cats after transient ischemia using dynamic magnetic resonance imaging. *Stroke* 1993;24:444–451.
41. Roberts TPL, Vexler Z, Derugin N, Moseley ME, Kucharczyk J. High-speed MR imaging of ischemic brain injury following stenosis of the middle cerebral artery. *J Cereb Blood Flow Metab* 1993;13:940–946.
42. Back T, Höhn-Berlage M, Kohno K, Hossmann K-A. Diffusion NMR imaging in experimental stroke: correlation with cerebral metabolites. *Stroke* 1994;25:494–500.
43. Gadian DG, Allen K, Bruggen Nvan, Busza AL, King MD, Williams SR. Applications of NMR spectroscopy to the study of experimental stroke in vivo. *Stroke* 1993;24(suppl I):I-57–I-59.
44. Monsein LH, Mathews VP, Barker PB, et al. Irreversible regional cerebral ischemia: serial MR imaging and proton MR spectroscopy in a nonhuman primate model. *AJNR* 1993;14:963–970.
45. Ter-Pogossian MM. PET, SPECT and NMRI: competing or complementary disciplines? *J Nucl Med* 1985;26:1487–1498.